BIOCHEMISTRY
including biophysical chemistry & molecular biology

Article

pubs.acs.org/biochemistry

Omecamtiv Mecarbil Modulates the Kinetic and Motile Properties of Porcine β-Cardiac Myosin

Yingying Liu,[†] Howard D. White,[†] Betty Belknap,[†] Donald A. Winkelmann,[‡] and Eva Forgacs*,[†]

[†]Department of Physiological Sciences, Eastern Virginia Medical School, Norfolk, Virginia 23507, United States

[‡]Department of Pathology and Laboratory Medicine, Robert Wood Johnson Medical School, Rutgers University, Piscataway, New Jersey 08854, United States

Supporting Information

ABSTRACT: We determined the effect of Omecamtiv Mecarbil, a novel allosteric effector of cardiac muscle myosin, on the kinetic and "*in vitro*" motility properties of the porcine ventricular heavy meromyosin (PV-HMM). Omecamtiv Mecarbil increases the equilibrium constant of the hydrolysis step (M-ATP ⇄ M-ADP-P_i) from 2.4 to 6 as determined by quench flow, but the maximal rates of both the hydrolysis step and tryptophan fluorescence increase are unchanged by the drug. OM also increases the amplitude of the fast phase of phosphate dissociation (AM-ADP-P_i → AM-ADP + P_i) that is associated with force production in muscle by 4-fold. These results suggest a mechanism in which hydrolysis of M-ATP to M-ADP-P_i occurs both before and after the recovery stroke, but rapid acceleration of phosphate dissociation by actin occurs only on post-recovery stroke A-M-ADP-P_i. One of the more dramatic effects of OM on PV-HMM is a 14-fold decrease in the unloaded shortening velocity measured by the *in vitro* motility assay. The increase in flux through phosphate dissociation and the unchanged rate of ADP dissociation (AM-ADP → AM + ADP) by the drug produce a higher duty ratio motor in which a larger fraction of myosin heads are strongly bound to actin filaments. The increased internal load produced by a larger fraction of strongly attached crossbridges explains the reduced rate of *in vitro* motility velocity in the presence of OM and predicts that the drug will produce slower and stronger contraction of cardiac muscle.

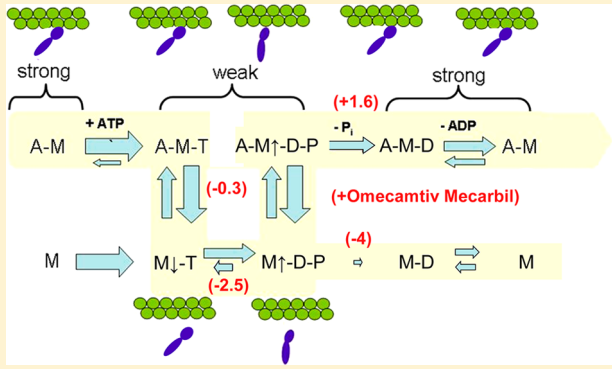

Heart failure represents one of the most pressing medical problems in the world affecting millions of people.[1,2] In the majority of cases, there is weakened systolic function because of the weakening of the heart. To preserve cardiac output, the body activates neurohormonal pathways causing cardiac remodeling that results in further weakening of the heart muscle and a decline in cardiac output.[3] Drugs available for the treatment of systolic dysfunction include positive inotropic agents such as β-adrenergic receptor agonists or inhibitors of phosphodiesterase activity.[4] These drugs increase the concentration of intracellular calcium, thus enhancing cardiac muscle contractility by extending the duration of the systolic ejection. Although effective, they have been linked to potentially life-threatening side effects such as ventricular arrhythmias, tachycardia, and hypotension, as well as increased rate of myocardial oxygen consumption and a reduced efficiency of energy utilization, factors that can cause worse patient outcomes and increase mortality.[5,6]

Recently, a large drug screen identified a novel small molecule, Omecamtiv Mecarbil (OM), that binds directly to cardiac muscle myosin and acts as an allosteric effector to stimulate motor activity and enhance cardiac performance without altering the intracellular calcium concentration.[7] Malik et al.[7] analyzed the action of OM on bovine β-cardiac S1 (subfragment 1) with reconstituted thin filaments to elucidate how the ATP hydrolysis mechanism is affected by OM. They found that it enhances the force-generating ability of myosin by accelerating the transition from weak to strong actin binding. The drug was evaluated in two different animal models and is in phase II clinical trials.[7−9] In animal models, OM was found to increase the stroke volume by extending the duration of systolic ejection and improving cardiac output.[9] This is a highly novel therapeutic approach, but a detailed kinetic mechanism of drug action on cardiac myosin has not been determined.

Cardiac myosin belongs to the class II family of conventional myosins.[10] In cardiomyocytes, myosin molecules form bipolar filaments and work as an assembly called the thick filament. The myosin molecules interact with the components of the thin filament (actin, tropomyosin, and troponin) to generate force. During the cardiac actomyosin crossbridge cycle, chemical energy from ATP hydrolysis is converted to mechanical energy.[10] ATP binds to myosin, and the actin-bound myosin head rapidly dissociates from actin followed by hydrolysis to M-ADP-P_i.

Received: December 12, 2014
Revised: February 6, 2015
Published: February 13, 2015

DOI: 10.1021/bi5015166
Biochemistry 2015, 54, 1963−1975

Binding of M-ADP-P_i to actin and P_i dissociation result in a conformational transition from a weak-binding AM-ADP-P_i to a strong-binding AM-ADP state. Release of phosphate is accompanied by a conformational change in the myosin head that produces an 8−10 nm power stroke and generates 3−6 pN of force.[11−15] ADP subsequently dissociates from the actomyosin-ADP to regenerate rigor actomyosin, thus returning to the beginning of the cycle.

Cardiac myosin is a dimer of myosin heavy chains that can be functionally divided into three major domains: an ATP and actin-binding region that comprise the so-called motor domain or head, a neck domain that binds the essential and regulatory light chains and acts as a semi-rigid lever arm, and a long α-helical coiled-coil tail domain that is essential for filament assembly. Vertebrates have two major cardiac myosin isoforms, α (fast) and β (slow). In large mammals (e.g., rabbits, pigs, and humans), β-cardiac myosin is the predominant isoform expressed in the ventricular muscle; it is also expressed in some slow skeletal muscle fibers. The α-cardiac myosin is present in the atria of the heart. In contrast, α-cardiac myosin is the predominant isoform in the ventricles of small mammals like mice and rats.[16]

Here we have used porcine ventricular heavy meromyosin (PV-HMM), a β-cardiac myosin isoform, to elucidate the precise mechanism of action of OM by steady-state and transient kinetic assays and *in vitro* motility experiments. We found that OM shifts the equilibrium of the hydrolysis step (M-ATP ⇄ M-ADP-P_i) and consequently accelerates the flux through the product dissociation steps from actomyosin-ADP-P_i. However, the rate of ADP dissociation from actomyosin is unchanged. This combination of changes in the kinetic mechanism leads to a higher concentration of strongly bound, force-producing cross-bridges and provides an explanation for the dramatic reduction in the unloaded shortening velocity measured by *in vitro* motility assays that is a consequence of an internal load imposed by the additional strongly bound intermediates.

MATERIALS AND METHODS

Reagents. Actin was purified from rabbit skeletal muscle.[17] Native porcine cardiac thin filaments were prepared according to the procedure of Spiess et al.[18] as modified by Matsumoto et al.[19] ATP and ADP were purchased from Sigma-Aldrich. Omecamtiv Mecarbil (CK-1827452) was purchased from Selleck Chemicals (http://Selleckchem.com). A 10 mM stock solution of OM was prepared in dimethyl sulfoxide (DMSO), and aliquots were stored at −80 °C. *N*-[2-(1-Maleimidyl)ethyl]-7-(diethylamino)-coumarin-3-carboxamide phosphate-binding protein (MDCC-PBP) was synthesized according to the method of Brune et al.[20] Porcine ventricular heavy meromyosin was prepared by chymotrypsin digestion according to a modification of the procedure by Siemankowski and Dreizen.[21] Digestion was stopped with trypsin inhibitor, and the protein was run on a Mono-Q ion exchange column to separate the S1 and HMM fragments; however, only HMM was used in this study. All preparations were analyzed on a 4 to 20% sodium dodecyl sulfate−polyacrylamide gel electrophoresis (SDS−PAGE) (Figure 1) to determine the integrity of the polypeptide chains. The lower molecular weight light chain (LC2) is clipped, which is also observed in the preparation of mammalian skeletal myosin HMM. Enzymatic activity was determined by steady-state ATPase assays (Figure 2).

Basal and Actin- and Thin Filament-Activated Steady-State ATPase Measurements. Steady-state ATPase activity was measured by an NADH coupled assay as described previously.[22] Addition of 0.5% DMSO had no effect on the rates. Measurements with thin filaments were taken at pCa <4 (100 μM Ca), pCa 6.6 (1 mM EGTA and 0.55 mM Ca), and pCa >8 (2 mM EGTA). The ATPase activity of the actin or the thin filaments alone was subtracted from the actomyosin data.

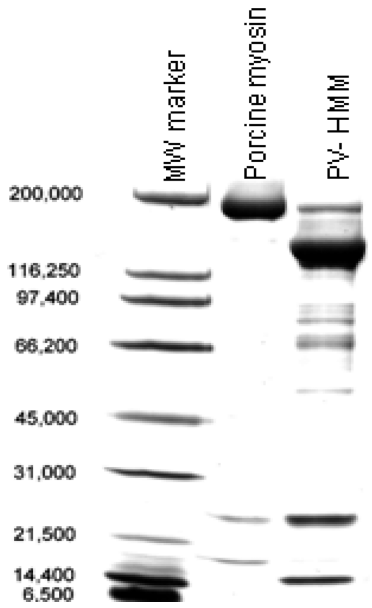

Figure 1. Purification of the porcine ventricular heavy meromyosin (PV-HMM). SDS−PAGE gel (4 to 20%) showing isolated porcine ventricular cardiac myosin and the chymotryptic PV-HMM fragment used for these studies.

Quench Flow Experiments. Chemical quench measurements were conducted using a computer-controlled stepper motor apparatus built in our laboratory[23] to drive syringes in a mixing unit from KinTek Corp. (Austin, TX). Solutions of PV myosin-HMM (15 μL) and ATP (10 μL containing 100000 dpm of [γ-^{32}P]ATP) were mixed, held in a delay line for the desired time, and then quenched by a second mix with 0.3 M KH_2PO_4 and 2 N HCl to give a final volume of 1.0 mL. The total radioactivity in each sample was determined by counting 0.3 mL of the sample directly. A 0.6 mL portion of the sample was mixed with an equal volume of a 10% (w/v) charcoal slurry and spun for 3 min at 10000 rpm in a tabletop Eppendorf centrifuge to remove unhydrolyzed ATP by binding to charcoal, and 0.6 mL of the supernatant solution was counted. The percent hydrolysis was obtained from the ratio of the radioactivity in charcoal-treated to directly counted samples after subtracting the background from each. One or two exponential functions were fit to the data using Simplex fitting routines in Scientist (Micromath, Ogden, UT) to obtain amplitude and rate information.

Stopped-Flow Experiments. All stopped-flow measurements were taken at 20 °C using an SF-2001 stopped-flow apparatus (KinTek Corp.) fit with two 2 mL syringes and one 5 mL syringe. In double-mixing experiments, myosin and ATP were mixed, allowed to incubate for the desired time, and then mixed with actin or thin filaments to give a 2/9 dilution of cardiac myosin and nucleotide and a 5/9 dilution of actin in the flow cell. Single-mixing experiments resulted in a 2/7 dilution of myosin and a 5/7 dilution of nucleotide or actin or thin filaments in the flow cell. The excitation light from a 75 W xenon lamp was selected by using a 0.2 m monochromator (Photon Technology International, South Brunswick, NJ). All experiments were

DOI: 10.1021/bi5015166
Biochemistry 2015, 54, 1963−1975

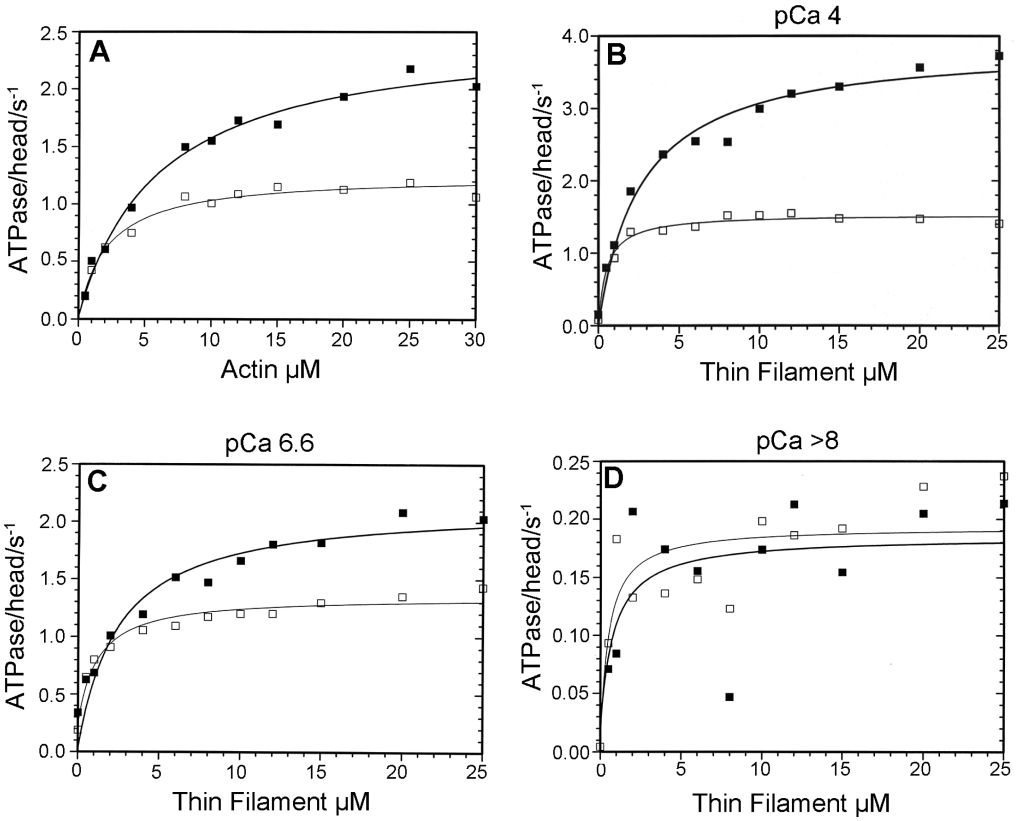

Figure 2. NADH-coupled actin and thin filament-activated ATPase assays. All steady-state ATPase rates were measured at 25 °C. Experiments were conducted in a buffer containing 4 mM MOPS, 2 mM $MgCl_2$, 0 mM KCl, and either 100 μM OM (□) or 0.5% DMSO (■) (pH 7.2). PV-HMM at 0.06 μM (active site concentration) was used to measure the ATPase activity over a range of actin (0−30 μM) or thin filament concentrations (0−25 μM). (A) The actin-activated ATPase had a V_{max} of 2.5 s^{-1} without and 1.3 s^{-1} with OM and K_{ATPase} values of 6 and 2.1 μM, respectively. (B) Values for thin filament-activated ATPase at pCa <4 were 3.9 s^{-1} without and 1.5 s^{-1} with OM. The K_{ATPase} values were 2.7 and 0.5 μM in the absence and presence of OM, respectively. (C) At pCa 6.6, the V_{max} was 1.8 s^{-1} in the absence and 0.97 s^{-1} in the presence of OM. The K_{ATPase} values were 3.1 and 0.8 μM, respectively. (D) At pCa >8, the V_{max} was ~0.2 s^{-1} and the K_{ATPase} <2 μM in the presence and absence of OM.

conducted in a buffer containing 5 mM MOPS and 2 mM $MgCl_2$ (pH 7.2) at 20 °C. All syringes contained either DMSO or DMSO + Omecamtiv Mecarbil. Some experiments were conducted without DMSO or OM. Light scattering was measured by using an excitation wavelength of 450 nm and a 400 nm long-pass filter. Tryptophan fluorescence experiments utilized excitation at 295 nm, and emission was selected with a 320−380 nm bandpass filter. The dissociation of phosphate from the actomyosin-ADP-P_i complex was measured using MDCC-PBP as described by White et al.[23] Background P_i was removed by including a phosphate mop consisting of 0.10 mM 7-methylguanosine and 0.02 unit/mL purine-nucleoside phosphorylase (Sigma, St. Louis, MO) in all of the reaction solutions. Actin or thin filaments and myosin solutions were extensively dialyzed (more than three times against 1000-fold buffer). The pH values of buffers used in phosphate dissociation experiments were adjusted by adding base to the buffer, after which a small sample of buffer was used to determine the pH and then discarded to avoid contaminating the buffer with phosphate from the pH electrode that is typically either stored in or calibrated with phosphate buffer.

Data Analysis and Kinetic Simulation. Three or four data sets of 1000 points were averaged, and the observed rate constants were obtained by fitting one- or two-exponential equations to the data using the software package included with the KinTek stopped-flow instrument. Scientist software was used to replot the data for publication and for kinetic simulations.[24]

***In Vitro* Motility Assays.** Porcine HMM was diluted to 40 μg/mL and bound to freshly prepared nitrocellulose-coated glass coverslips by incubation for 5 min at 22 °C. The surfaces were then blocked with 1% bovine serum albumin in PBS for 5 min, transferred to assay buffer, and held at 4 °C until they were assayed. Motility is measured in an assay chamber in motility buffer containing 1 nM phalloidin-rhodamine labeled actin as previously described.[25] To titrate the effect of the drug on motility, a stock of Omecamtiv Mercarbil (2.5 mM in DMSO) was diluted with DMSO and added to motility buffer containing phalloidin actin to obtain the indicated concentration of the drug (from 0 to 12.5 μM) and a constant concentration of 0.5% DMSO. Addition of 0.5% DMSO to the assay buffer had no effect on motility in the absence of drug. The chamber is observed with a temperature controlled stage and objective set at 32 °C on an upright microscope with an image-intensified CCD camera capturing data to an acquisition computer at 5−30 frames/s depending on the assay parameters. Movement of actin filaments from 500 to 1000 frames of continuous imaging is analyzed with semiautomated filament tracking programs.[25−27] The trajectory of every filament with a lifetime of at least 10 frames is determined. The instantaneous velocity of the filament moving along the trajectory, the filament length, the distance of continuous motion, and the duration of pauses are tabulated. A weighted probability of the actin filament velocity for hundreds of events is fit to a Gaussian distribution and reported as a mean velocity and standard deviation (SD) for each experimental condition.

DOI: 10.1021/bi5015166
Biochemistry 2015, 54, 1963−1975

RESULTS

Steady-State Basal, Actin- and Thin Filament-Activated ATPase. To investigate the effect of OM on the steady-state ATPase activity, we measured the dependence of the ATPase activity of porcine cardiac myosin HMM on actin or native thin filament (TF) concentrations with or without 100 μM OM (Figure 2). The addition of OM decreased the V_{max} of actin-activated ATPase activity of PV-HMM from 2.5 to 1.3 s^{-1}. OM also lowered the K_{ATPase} for actin activation ~3-fold from 6 μM in its absence to 2.1 μM and decreased the V_{max} of native thin filament-activated ATPase activity from 1.8 to 0.97 s^{-1} at pCa 6.6 (intermediate activation) and from 3.9 to 1.5 s^{-1} at pCa <4 (full activation) (Table 1). There was a 3.5-fold decrease in the K_{ATPase} for thin filament activation from 3.1 to 0.8 μM at pCa 6.6 and from 2.7 to 0.5 μM (5-fold) at pCa <4 in the presence of OM. We did not see an OM-induced increase in the V_{max} of actin- or thin filament-activated ATPase for PV-HMM under these assay conditions or under the assay conditions originally reported for bovine cardiac S1.[7] There were essentially no differences in the V_{max} or K_{ATPase} (~0.2 s^{-1} or <2 μM, respectively) of thin filament-activated ATPase rates at pCa >8 in the presence or absence of OM. Steady-state ATPase experiments were also conducted at an additional series of calcium concentrations between pCa 5 and 8 (Figure 1 of the Supporting Information).

Table 1. Steady-State Kinetic Parameters Measured by a NADH-Coupled Assay

process	rate constant	value: without OM	value: with OM
basal steady state	k_{Basal} (s^{-1})	0.017 ± 0.0005	0.004 ± 0.0005
basal steady state (quenched flow)	k_{-DP} (s^{-1})	0.022 ± 0.002	0.006 ± 0.002
actin-activated steady state	V_{max} (s^{-1})	2.5 ± 0.09	1.3 ± 0.05
	K_{ATPase} (μM)	6 ± 0.67	2.1 ± 0.37
thin filament-activated steady state, pCa 4	V_{max} (s^{-1})	3.9 ± 0.11	1.5 ± 0.06
	K_{ATPase} (μM)	2.7 ± 031	0.5 ± 0.15
thin filament-activated steady state, pCa 6.6	V_{max} (s^{-1})	1.8 ± 0.07	0.97 ± 0.04
	K_{ATPase} (μM)	3.1 ± 0.48	0.8 ± 0.19
thin filament-activated steady state, pCa >8	V_{max} (s^{-1})	0.2 ± 0.02	0.2 ± 0.02
	K_{ATPase} (μM)	<2	<2

The steady-state results are summarized in Table 1. In the absence of actin or thin filaments, OM produced a significant decrease in the basal steady-state ATPase activity of PV-HMM from 0.017 to 0.004 s^{-1} as previously reported.[7] The OM concentration dependence of steady-state ATPase of the PV-HMM rates was used to determine a K_I of 0.27 μM for allosteric inhibition by OM (Figure 2 of the Supporting Information). In the presence of actin or thin filaments at pCa ≤6.6, both the steady-state rates and the K_{ATPase} are reduced by OM. The smaller K_{ATPase} measured in the presence of OM indicates either a higher affinity of M-ADP-P_i for actin, and thin filaments at pCa 4.0 and 6.6 or may only be due to an apparent increase in the affinity resulting from a slower rate-determining step.

Transient Kinetics. We used transient kinetic experiments to assess the effects of OM on the individual steps of the mechanochemical cycle. Scheme 1 illustrates elemental steps of the actomyosin ATPase cycle highlighting the steps measured by stopped-flow and quench flow kinetic assays.

Scheme 1. Minimal Kinetic Scheme of the ATPase Cycle[a]

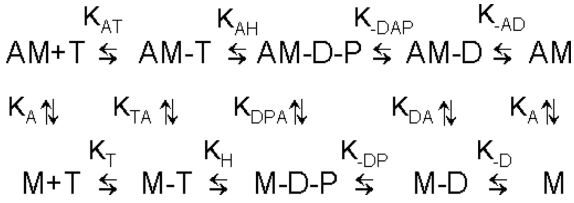

[a]Abbreviations: A, actin; M, PV-HMM; T, ATP; D, ADP; P, phosphate. Positive subscripts denote the binding of the last ligand in the subscript, and negative subscripts denote dissociation (rate constants are similarly identified throughout the manuscript, e.g., k_{-AD} the rate of dissociation of ADP from actoPV-HMM-ADP).

Dissociation of PV-HMM from Actin upon ATP Binding (AM + ATP ⇄ AM-ATP → A + M-ATP). Scheme 1 illustrates an elementary mechanism, which can represent rapid ATP binding followed by dissociation of M-ATP, but a more likely mechanism includes ATP binding, followed by a change in the conformation of the myosin that results in reduced affinity and rapid dissociation of the M-ATP from actin. The rate of dissociation of PV-HMM from actin in the presence of ATP was measured by light scattering after mixing actoPV-HMM with increasing concentrations of ATP in the presence or absence of OM (Figure 3). In the presence of OM, the rapid decrease in light scattering was sometimes followed by a slow increase in light scattering with amplitudes typically less than 10% and k_{obs} values of 0.5−5 s^{-1}. However, the rate constants measured for the slow phase were erratic and did not show a consistent dependence upon ATP concentration and were therefore not analyzed further. The fast phase data were fit by a maximal rate (k_{-TA}) of 941 s^{-1} and a K_{AT} of 128 μM in the absence of OM. The drug decreased the dissociation rate by 1.4-fold to 655 s^{-1} with little change in K_{AT} (117 μM) (Figure 3C). The second-order rate constants calculated from the initial slopes were 7.4 μM^{-1} s^{-1} in the absence and 5.6 μM^{-1} s^{-1} in the presence of OM, the difference being similar (1.3-fold slower) to the difference observed in the maximal rate (Figure 3D). As has been shown for other actomyosins, the rate of dissociation by ATP is much faster than any of the steps in the pathway with or without drug.[21]

ATP Binding and Hydrolysis (M + ATP → M-ATP ⇄ M-ADP-P_i → M). β-Cardiac myosin has a tryptophan residue (W508) in its relay loop that acts as an intrinsic fluorescence sensor of conformational changes required for ATP hydrolysis.[28−30] The enhancement of the intrinsic tryptophan fluorescence intensity was used to measure ATP binding and hydrolysis (Figure 4). Porcine ventricular HMM was mixed with ATP in single-mixing stopped-flow fluorescence measurements with or without OM (Figure 4A,B). The dependence of the rate of fluorescence increase versus ATP concentration was fit to a hyperbolic equation. There was no significant difference in the maximal rate of fluorescence enhancement measured without OM ($k_H + k_{-H}$ = 71 s^{-1}, and K_T = 24 μM) or with OM ($k_H + k_{-H}$ = 80 s^{-1}, and K_T = 22 μM) (Figure 4C). The second-order rate constant for ATP binding (k_T) was 3 μM^{-1} s^{-1} in the absence and 3.6 μM^{-1} s^{-1} in the presence of OM. OM increases the fluorescence signal approximately 20% in the absence of ATP [t = 0 (Figure 4A,B)]. OM also increases the amplitude of the fluorescence signal by almost 2-fold at >300 μM ATP (Figure 4D). This would occur if there is a shift in the hydrolysis equilibrium in Scheme 1 from M-ATP toward a

DOI: 10.1021/bi5015166
Biochemistry 2015, 54, 1963−1975

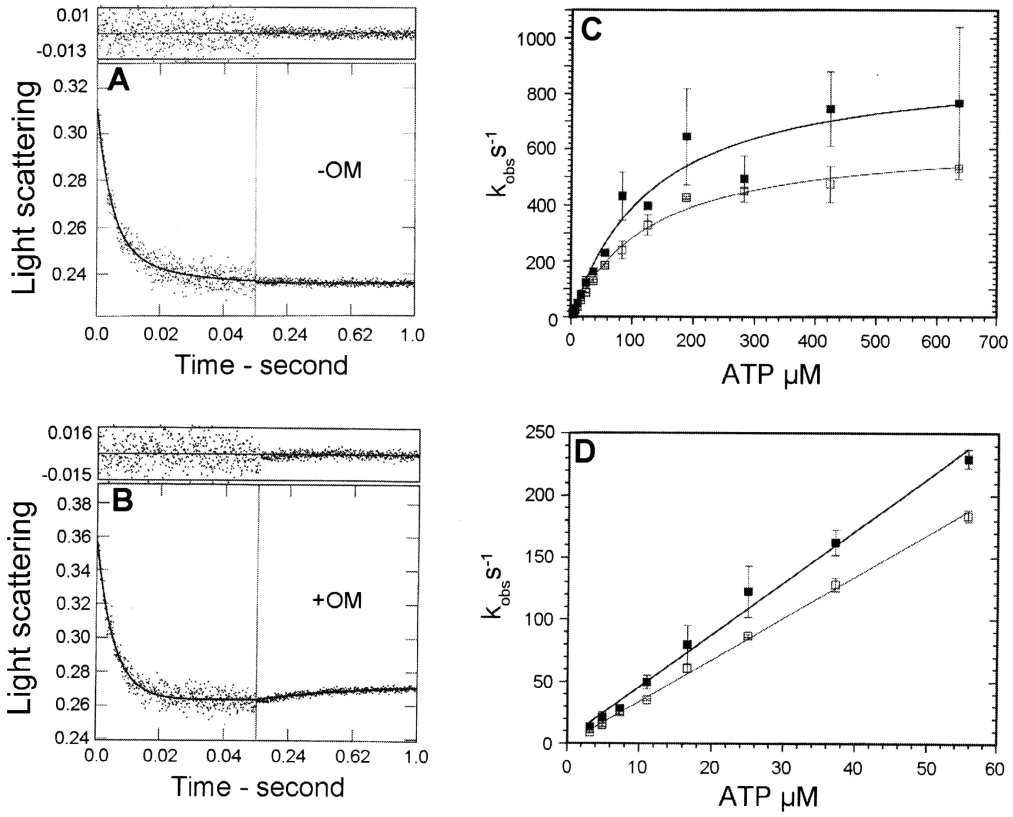

Figure 3. ATP-induced dissociation of PV-HMM from actin. A decrease in light scattering was observed upon mixing 3 μM actoPV-HMM with increasing concentrations of MgATP. Experimental conditions in the cell: 0.86 μM actoPV-HMM, 3.2−636 μM ATP, 5 mM MOPS (pH 7.2), 2 mM $MgCl_2$, 25 mM KCl, 0.125% DMSO, and either 0 (■) or 25 μM OM (□) at 20 °C. Three traces were averaged and fit to a one- or two-exponential equation. Representative traces at 56 μM ATP yielded (A) $I(t) = 0.056e^{-221t} + C$ in the absence of OM and (B) $I(t) = 0.096e^{-179.1t} - 0.01e^{-1.45t} + C$ in the presence of OM. (C) Dependence of k_{obs} of the fast phase on ATP concentration fit to a hyperbola [$k_{obs} = k_{-TA}/(1 + K_{app}/[ATP])$], resulting in a k_{-TA} of 941 ± 60 s^{-1} and a K_{app} of 128 ± 29 μM in the absence (■) and values of 655 ± 56 s^{-1} and 117 ± 38 μM, respectively, in the presence of 25 μM OM (□). (D) Data from 3.2−56 μM ATP. The second-order rate constants for ATP binding to actoPVHMM calculated from the initial slopes are as follows: k_{AT} = 7.4 μM^{-1} s^{-1} in the absence of OM, and k_{AT} = 5.6 μM^{-1} s^{-1} in the presence of OM.

high-fluorescence M-ADP-P_i intermediate. The amplitudes of the increase in fluorescence (Figure 4D) decrease with an increasing ATP concentration, because the signal from an initial second-order binding step (not shown) is probably being lost in the dead time of the stopped flow.[31]

Quench Flow Measurements of Pre-Steady-State ATP Hydrolysis (M + ATP → M-ATP ⇄ M-ADP-P_i → M-ADP → M). Because the results of the tryptophan fluorescence measurements indicated a shift in the equilibrium toward hydrolysis mediated by OM, we used quenched flow to directly measure ATP hydrolysis to determine the rate and equilibrium constants (k_H, k_{-H}, and K_H) of the hydrolysis step. The experiments shown in Figure 5 were conducted by mixing the PV-HMM with ATP in the presence or absence of OM for the indicated times before quenching the reaction with acid. The data in Figure 5A were determined under conditions in which [HMM] > [ATP], and the observed rate of hydrolysis was limited by the rate of binding of ATP to HMM. For all myosin isoforms studied thus far, rapid and irreversible binding of ATP to the active site is followed by rapid hydrolysis and subsequently by slow (rate-limiting) dissociation of phosphate (M + ATP → M-ATP ⇄ M-ADP-P_i → M-ADP + P_i). The fraction of ATP hydrolysis as a function of incubation time (Figure 5A) was best fit by two-exponential equations. The rates of the initial more rapid phase of hydrolysis are associated with the formation of M-ADP-P_i, which releases P_i with the acid quench, and the second slower phase measures the decay of M-ATP at the rate of phosphate dissociation. The ratio of the amplitudes provides a direct measurement of the hydrolysis equilibrium constant $K_H = A_{fast}/A_{slow}$, which equals 2.4 in the absence of OM and 6 in the presence of OM. These data indicate that the equilibrium is shifted further toward hydrolysis (M-ADP-P_i) by the drug. The rates of the slow phases of 0.019 s^{-1} without OM and 0.006 s^{-1} with OM are in good agreement with the basal steady-state ATPase rates (0.017 and 0.004 s^{-1}, respectively) measured by the NADH-coupled assay (Table 1). When the PV-HMM was incubated with ATP under conditions in which ATP binding is rapid and [ATP] > [M], the initial rapid component was 56 s^{-1} in the presence of OM and 55 s^{-1} in the absence of OM (Figure 5B). These results show that the hydrolysis is rapid, but the maximal rate was not significantly altered by OM. The rates observed here by quench flow are similar to those observed by the tryptophan fluorescence experiments at the same ATP concentration as shown in Figure 4. The maximal extrapolated rates obtained by tryptophan fluorescence and the K_H obtained by quench flow can be used to obtain the forward and reverse rate constants of hydrolysis in the absence of OM (k_H = 50 s^{-1}, and k_{-H} = 21 s^{-1}, respectively) and in the presence of OM (k_H = 69 s^{-1}, and k_{-H} = 11 s^{-1}, respectively). The maximal values measured by quench flow can be used to calculate k_H = 39 s^{-1} and k_{-H} = 16 s^{-1} in the absence of OM and k_H = 48 s^{-1} and k_{-H} = 6 s^{-1} in the presence of OM. There is a relatively small increase in

DOI: 10.1021/bi5015166
Biochemistry 2015, 54, 1963−1975

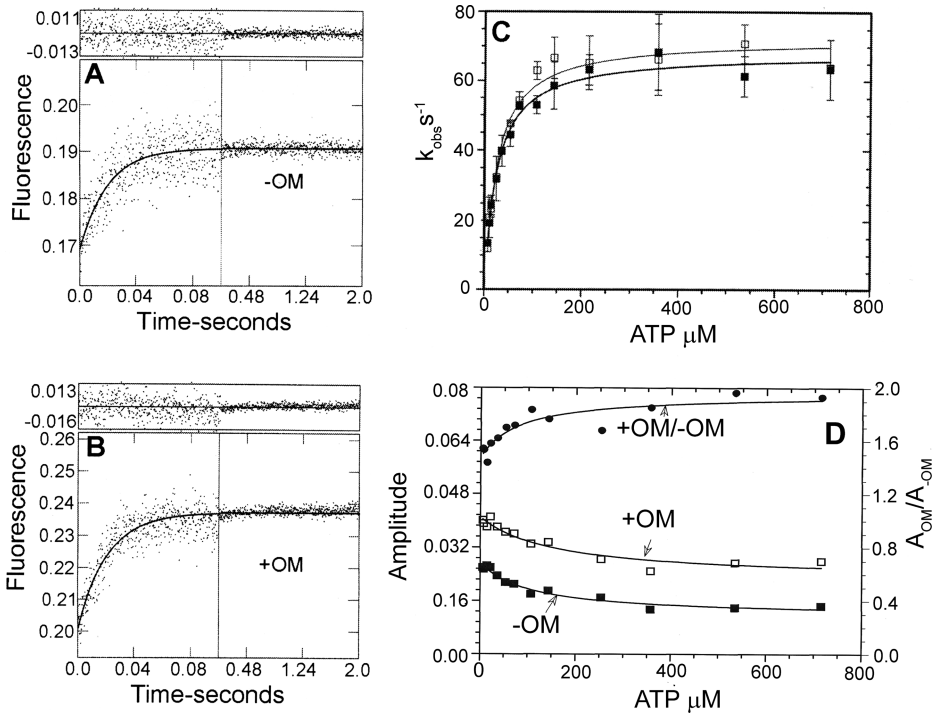

Figure 4. ATP binding to PV-HMM measured by tryptophan fluorescence. PV-HMM (10 μM) was mixed with increasing concentrations of ATP at 20 °C. Final concentrations in the cell were 2.9 μM PV-HMM, 7.1−714 μM ATP, 5 mM MOPS (pH 7.2), 2 mM $MgCl_2$, 25 mM KCl (pH 7.2), 0.25% DMSO, and either 0 (■) or 50 μM OM (□). Three traces for each ATP concentration were averaged and fit to a single-exponential equation. One-exponential fits of data obtained at 54 μM ATP in the cell yielded (A) $I(t) = 0.021e^{-51.4t} + C$ in the absence of OM and (B) $I(t) = 0.037e^{-48.1t} + C$ in the presence of OM. (C) Fit of the data obtained from 7.14 to 714 μM ATP to a hyperbola $[k_{obs} = k_{max}/(1 + [ATP]/K_{ATP})]$ yielded a maximal rate constant of $k_H + k_{-H}$ of 70.8 ± 5.1 s^{-1} and a K_{ATP} of 24 ± 5.7 μM in the absence of OM and a $k_H + k_{-H}$ of 80 ± 5.6 s^{-1} and a K_{ATP} of 21.8 ± 4.8 μM in the presence of OM. The second-order rate constants for binding of ATP to myosin were 3 μM^{-1} s^{-1} in the absence and 3.6 μM^{-1} s^{-1} in the presence of OM. (D) Dependence of the amplitudes of the tryptophan fluorescence enhancement with (□) and without (■) OM: $A(ATP) = A_o - A_{ATP}/(1 + K_{app}/[ATP])$. A_o is the fluorescence amplitude where there is no signal loss in the mixing time at low ATP concentrations; A_{ATP} is the fast change lost at high ATP concentrations, and $A_o - A_{ATP}$ is the amplitude of the signal from the recovery stroke that is insensitive to ATP concentration. The values fit for A_o and A_{ATP} are 0.041 and 0.018 in the presence of OM and 0.027 and 0.016 in the absence of OM, respectively. The ratio of the amplitudes of the fluorescence enhancement of the component that is sensitive to ATP concentration ($A_{o+OM}/A_{o-OM} = 0.018/0.016 = 1.12$) shows a relatively small increase with OM. At >300 μM ATP, the ratio of the amplitudes in the presence and absence of OM, A_{+OM}/A_{-OM} (●), approaches 1.95.

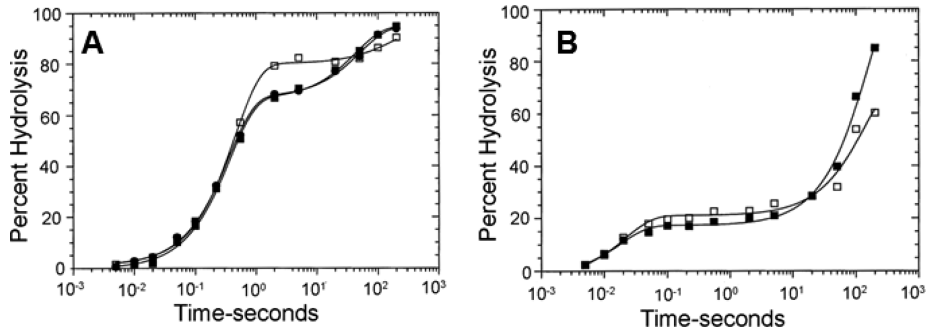

Figure 5. Determination of the hydrolysis equilibrium constant (K_H) by quenched flow. PV-HMM was mixed with ATP at 20 °C in buffer containing 0.75% DMSO without OM (■) or with 75 μM OM (□) without DMSO (●) and allowed to react for the indicated time and then quenched in acid. (A) Final concentrations in the delay line were 2.5 μM PV-HMM and 0.5 μM ATP, 5 mM MOPS (pH 7.2), 2 mM $MgCl_2$, and 25 mM KCl (pH 7.2). The solid lines through the data were best fit by double-exponential equations: $I(t) = 100 - (79e^{-2.3t} + 14e^{-0.006t})$ for 75 μM OM and $I(t) = 100 - (66e^{-2.85t} + 27e^{-0.019t})$ without OM and a control $I(t) = 100 - (66e^{-2.7t} + 28e^{-0.022t})$ without DMSO or OM. K_H (A_{fast}/A_{slow}) is 6 with 75 μM OM and 2.4 without DMSO and control. (B) Final concentrations in the delay line were 25 μM PV-HMM (heads) and 100 μM ATP. The solid lines through the data are the best fits to double-exponential equations: $I(t) = 100 - (23e^{-56t} + 80e^{-0.0086t})$ for 75 μM OM (□) and $I(t) = 100 - (19e^{-55t} + 83e^{-0.067t})$ (■) for the DMSO control.

k_H with OM, and most of the change in K_H is due to a decrease in k_{-H}.

Dissociation of ADP from ActoPV-HMM (AM + ADP ⇄ AM-ADP ⇄ AM + ATP → A + M-ATP). The rate of ADP dissociation from actoPV-HMM can be measured by the decrease in light scattering after mixing ATP with actoPV-HMM-ADP (Figure 6A,B). Dissociation of actoPV-HMM by ATP is limited by the rate of ADP dissociation. The dependence of k_{obs} upon ATP concentration was fit to a hyperbolic equation with a maximal rate k_{-AD} of 83 s^{-1} and a K_{app} of 61 μM ATP in the

DOI: 10.1021/bi5015166
Biochemistry 2015, 54, 1963−1975

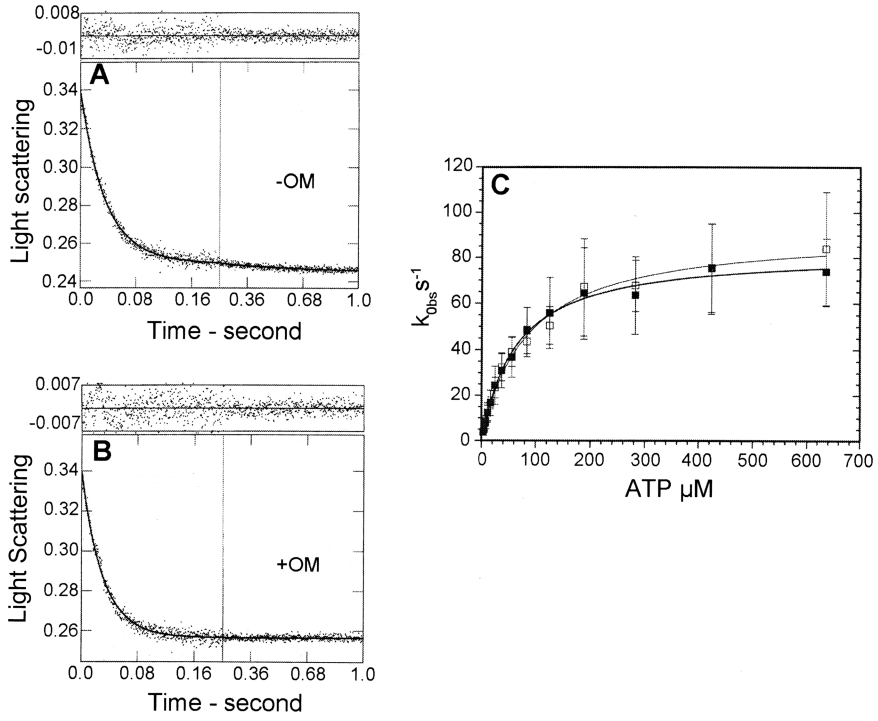

Figure 6. Dissociation of ADP from actoPV-HMM by ATP. The decrease in light scattering was observed at 20 °C upon mixing 3 μM actoPV-HMMADP (3 μM active sites and 6 μM actin, 100 μM ADP) with ATP. Final concentrations in the cell were 0.86 μM actoPVHMM, 3.2–636 μM ATP, 28.6 μM ADP, 5 mM MOPS (pH 7.2), 2 mM $MgCl_2$, 25 mM KCl, 0.125% DMSO, and either 0 (■) or 25 μM OM (□) at 20 °C. Three traces were averaged and fit to a single-exponential equation. (A) Representative trace showing the observed change in light scattering upon mixing 0.86 μM actoPV-HMMADP with 56 μM ATP in the absence of OM with a fit of $I(t) = 0.088e^{-27.9t} + C$. (B) A fit of $I(t) = 0.084e^{-32.8t} + C$ in the presence of 25 μM OM. (C) The dependence of k_{obs} on ATP concentration was fit to a hyperbola [$k_{obs} = k_{-AD}/(1 + K_{app}/[ATP])$], resulting in a maximal k_{-AD} of 83.1 ± 2.2 s^{-1} and a K_{app} of 61 ± 7.2 μM without OM and a k_{-AD} of 90 ± 2.4 s^{-1} and a K_{app} of 85.1 ± 9.7 μM with OM.

absence of OM and a k_{-AD} of 90 s^{-1} and a K_{app} of 85 μM in the presence of OM (Figure 6C). These results indicate that OM does not significantly alter the rate of dissociation of ADP from actoPV-HMM-ADP. The decrease by ADP of the apparent second-order rate constant k_{-TA} of ATP-dependent dissociation of actoPV-HMM can be used to calculate the rate, k_{AD}, and equilibrium, K_{AD}, constants of binding of ADP to acto-PVHMM[32] [$k_{AT(D)} = k_{AT}/(1 + [ADP]K_{AD})$].[22] The equilibrium constants calculated for K_{-AD} are 22 μM in the absence and 23.8 μM in the presence of OM. The rate constants calculated for ADP binding ($k_{AD} = K_{-AD}/k_A$) are calculated to be 3.7 μM^{-1} s^{-1} in the absence and 3.8 μM^{-1} s^{-1} in the presence of OM, which are indistinguishable within experimental error.

Phosphate Release (M-ADP-P_i + A ⇄ AM-ADP-P_i → AM-ADP + P_i). The release of phosphate from the active site of actomyosin-ADP-P_i is a key step in the transition from a weak to strong actin-binding interaction that is associated with the power stroke during the ATPase cycle. Fluorescently labeled phosphate-binding protein (MDCC-PBP) was used to monitor dissociation of phosphate from the (TF) PV-HMM-ADP-P_i complexes. In a double-mixing stopped-flow experiment, PV-HMM was first mixed with ATP under single-turnover conditions and incubated for 1 s to allow ATP binding and hydrolysis to occur, followed by mixing with actin to measure the rate of phosphate release. The rate of phosphate dissociation increases linearly with actin concentration to ~5 times the steady-state rate, but we could not obtain a maximal rate with actin (data not shown). Thin filaments were subsequently used instead of actin in these experiments because they are less viscous and M-ADP-P_i binds more tightly to thin filaments than to actin, which allowed us to determine the maximal rate of phosphate dissociation. Two phases were observed, and the observed rate constants were plotted against the thin filament concentration in the absence and presence of OM (Figure 7A,B). The fast phase resulted in an extrapolated maximal rate of phosphate dissociation (k_{-DAP}) of 17 s^{-1}, and the K_{TF} was 7.3 μM in the absence of OM; values of 28 s^{-1} and 7.9 μM, were found in the presence of OM, indicating that OM accelerates dissociation of phosphate from the (TF) PV-HMM-ADP-P_i complex (Figure 7C). The maximal rates for the slow phase were 0.4 s^{-1} without OM and 1 s^{-1} with OM. We had previously observed that the slow phase of phosphate dissociation at saturating actin was equal to the steady-state rate of ATP hydrolysis by fast rabbit skeletal actomyosin-A1S1 and suggested that "attached hydrolysis" was the rate-limiting step.[23] However, this is not the case for porcine cardiac actomyosin-HMM. Here the rate constants measured for the slow phase of phosphate dissociation are slower than the steady-state rates.

The fraction of the amplitudes of the fast phase ($A_{fast}/A_{fast} + A_{slow}$) is ~4 fold higher in the presence of OM (Figure 7D), which suggests that the hydrolysis is shifted toward the M-ADP-P_i intermediate (M-ATP ⇄ M-ADP-P_i), and consequently, more (TF) PV-HMM-ADP-P_i intermediate is being produced, leading to an increase in the flux through the phosphate release step. It is noteworthy that the phosphate release is not the rate-limiting step of the actomyosin cycle because it is ~5-fold faster than the steady-state ATPase rate. This finding was also reported by Houmeida et al.[33] The transient kinetic data are summarized in Table 2.

***In Vitro* Motility.** The unloaded shortening velocity of actin filament movement was determined with the *in vitro* motility

DOI: 10.1021/bi5015166
Biochemistry 2015, 54, 1963–1975

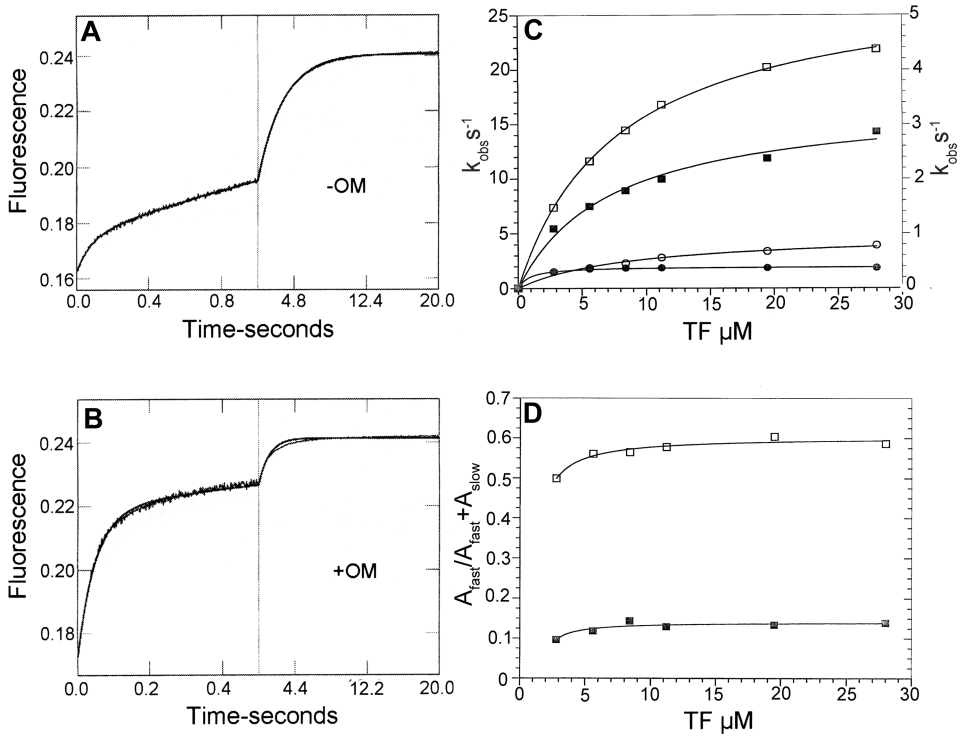

Figure 7. Kinetics of phosphate dissociation from TF-activated PV-HMM. Double-mixing stopped-flow experiments were performed using MDCC-PBP as described in Materials and Methods. PV-HMM (10 μM, sites) was first mixed with 5 μM ATP, held in a delay line for 2 s, and then mixed with thin filaments to accelerate P_i release. Final concentrations in the flow cell were 2.2 μM PV-HMM, 1.1 μM ATP, 0–28 μM TF, 5 mM MOPS, 2 mM $MgCl_2$, 0 mM KCl, 0.11 mM $CaCl_2$, 0.125% DMSO, either 0 (■) or 25 μM OM (□), 5 μM MDCC-PBP, 0.1 mM 7-methylguanosine, and 0.01 unit/mL purine nucleoside phosphorylase (pH 7.2) at 20 °C. Representative traces showing the change in fluorescence with 19.4 μM TF in the absence of OM. The data were fit to a double-exponential equation with (A) a fit of $I(t) = 0.012e^{-11.9t} + 0.06e^{-0.37t} + C$ and (B) a fit of $I(t) = 0.046e^{-20.2t} + 0.02e^{-0.9t} + C$ in the presence of 25 μM OM. (C) Three traces for each TF concentration were averaged and fit to a two-exponential equation. The hyperbolic fit [$k_{obs} = k_{-DAP}/(1 + K_{TF}/[TF])$] for the fast phase resulted in k_{-DAP} and K_{TF} values of 17 s^{-1} and 7.3 μM without OM (■) and 28 s^{-1} and 7.9 μM with 25 μM OM (□), respectively. The maximal rates for the slow phase were 0.4 s^{-1} in the absence of OM (●) and 1 s^{-1} in the presence of OM (○). (D) The fraction of the amplitude of the fast phase and slow phase ($A_{fast}/A_{fast} + A_{slow}$) is ~4-fold higher in the presence of 25 μM OM (□) than in the absence of the drug (■).

Table 2. Summary of Transient Kinetic Parameters

					Malik et al.[a]	
process	method	rate constant	without OM	with OM	without OM	with OM
ADP dissociation	SF light scattering	k_{-AD} (s^{-1})	83 ± 2.2	90 ± 2.4	66[b]	63[b]
ADP binding	SF light scattering	K_{AD} (μM)	22.2 ± 4	23.8 ± 5	ND[f]	ND[f]
ADP binding	SF light scattering	k_{AD} (μM^{-1} s^{-1})	3.7 ± 2	3.8 ± 3	ND[f]	ND[f]
dissociation of AM by ATP	SF light scattering	k_{-TA} (s^{-1})	941 ± 60	655 ± 56	~90[c]	~90[c]
ATP binding to AM	SF light scattering	k_{AT} (μM^{-1} s^{-1})	7.4 ± 1	5.6 ± 0.6	ND[f]	ND[f]
ATP hydrolysis	SF tryptophan fluorescence	$k_H + k_{-H}$ (s^{-1})	71 ± 5	80 ± 6	ND[d,f]	ND[d,f]
ATP binding	SF tryptophan fluorescence	k_T (μM^{-1} s^{-1})	3.0 ± 0.4	3.6 ± 0.6	ND[f]	ND[f]
ATP hydrolysis	quenched flow	$k_H + k_{-H}$ (s^{-1})	55 ± 8	56 ± 10	ND[f]	ND[f]
ATP hydrolysis	quenched Flow	K_H	2.4 ± 0.5	6 ± 1	ND[f]	ND[f]
P_i release (no actin)	MDCC-PBP	k_{-DP} (s^{-1})	0.02 ± 0.004	0.004 ± 0.004	0.032	0.004
P_i release	MDCC-PBP	k_{-DAP} (s^{-1})	17 ± 1	28 ± 1	2.4[e]	9.2[e]
P_i release	quenched flow	k_{-DP} (s^{-1})	0.019 ± 0.002	0.006 ± 0.002	ND[f]	ND[f]
in vitro motility	*in vitro* motility assays	μm/s	0.96 ± 0.23	0.07 ± 0.01	ND[f]	ND[f]

[a]Data from ref 7. [b]Maximal rate of ADP dissociation measured with deacADP as the substrate at a single ATP concentration (1 mM). [c]The measured rates are similar to the rates of ADP release, which is probably due to the myosin having ADP bound to its active site. [d]Single traces are shown at a single ATP concentration (1 μM); maximal rates not determined. [e]Actin-dependent P_i release was determined at a single actin concentration (14 μM). [f]Not determined.

assay. The PV-HMM was bound directly to nitrocellulose coated coverslips, and actin filament movement was recorded and analyzed. The actin filament velocity for porcine HMM was 0.96 μm/s (Figure 8A). The filament movement is often interrupted by pauses consistent with filament trapping on point defects on the surfaces (Figure 3 of the Supporting Information). Pinned filaments exhibit undulating or spiral rotational motion and often escape from the defect after a residence time that is temperature-dependent.[25] This results in a rather broad velocity distribution for the porcine HMM without OM. The speed is

DOI: 10.1021/bi5015166
Biochemistry 2015, 54, 1963–1975

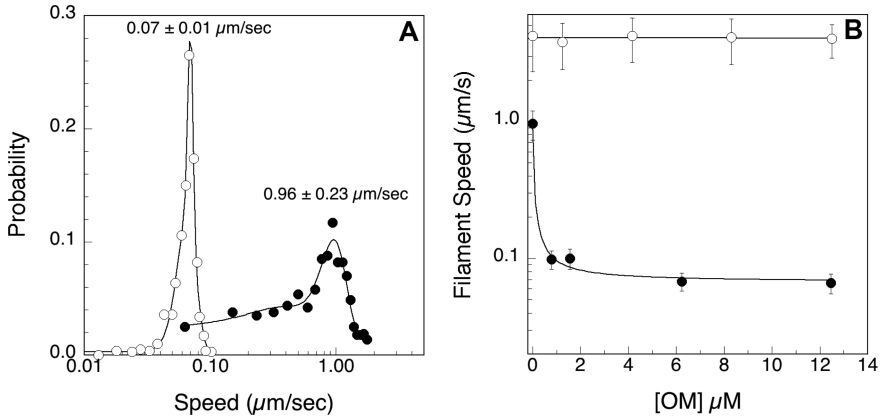

Figure 8. *In vitro* motility assay. (A) Unloaded shortening velocity distribution for actin filaments moving on PV-HMM in the presence of 12.5 μM OM (○). Untreated PV-HMM moves actin filaments at a mean velocity of 0.96 ± 0.25 μm/s (●). The velocity is broadly distributed with filament motion often interrupted by pauses caused by trapping on surface point defects. Addition of OM dramatically slows the velocity of the actin filaments to 0.07 ± 0.01 μm/s, and the filament motion becomes more uniform and continuous with long periods of uninterrupted movement at the slower speed. (B) Titration curve for the effect of OM on the motor activity of PV-HMM (●). The apparent K_D for OM binding is 0.2 μM. As a control, skeletal myosin from chicken pectorals major was titrated with OM (○). The fast striated muscle myosin moves actin filaments at a rate of 4.1 ± 1.5 μm/s, and OM has little effect on filament velocity. Assays were conducted at 32 °C. The filament speed is presented on a log scale for both panels A and B.

consistent with the detachment-limited model for unloaded shortening velocity in which 7 nm steps[34] were limited by ADP dissociation (7 nm × 200 s^{-1} = 1.4 μm/s). The rate of ADP dissociation measured here at 20 °C, 83 s^{-1}, is estimated to be ~200 s^{-1} at 32 °C based on a Q10 of ~2 determined for dissociation of ADP from bovine cardiac actomyosin.[32] The addition of OM had two significant effects. There was a dramatic decrease in filament velocity (>14-fold at saturation), and the filament motion became more continuous with long periods of uninterrupted movement at the slower speed (Figure 3 of the Supporting Information). Similar values of the OM effect on *in vitro* motility were obtained recently by Wang et al.[35] This suggests that drug binding results in greater forces per filament overcoming the pinning defects that can trap actin filaments in the motility assay. The slower rate of movement in the presence of OM was unexpected but may be explained by resistance to rapid filament movement resulting from a larger number of crossbridges in strongly bound AM-ADP intermediates. Titration with increasing concentrations of OM resulted in an apparent K_I of ~0.2 μM, consistent with the value measured for inhibition of the steady-state ATPase activity (Figure 2 of the Supporting Information). OM had no effect on velocity or an enhancement of the persistence of filament movement of chicken skeletal muscle myosin that was used as a control. This is consistent with the reported selectivity of the drug[7] (Figure 8B).

DISCUSSION

Here we report how the novel cardiac myosin drug, Omecamtiv Mecarbil, alters the ATP hydrolysis mechanism and *in vitro* motility of porcine ventricular HMM (PV-HMM). The steady-state rate of thin filament-activated ATPase of PV-HMM was 2−3-fold lower at high calcium concentrations (pCa <4), 1.5-fold lower at an intermediate calcium concentration (pCa 6.6), and not altered at low calcium concentrations (pCa >8) by the drug (Figure 2 and Table 1). This is in contrast to the published data[7] that report an increase in thin filament-activated ATPase rates at intermediate to low calcium concentrations. However, the published experiments were conducted at only a single thin filament concentration, and the maximal ATPase rate was not determined. OM decreases the basal steady-state ATPase rate of the PV-HMM by 2−3-fold in both steady-state (Table 1) and single-turnover experiments (Figure 5A). Dissociation of phosphate from cardiac and skeletal actomyosin ADP-P_i is 5−10 fold faster than the steady-state rate and is therefore not rate limiting. We have not been able to identify the kinetic step that limits the steady-state rate of ATP hydrolysis at saturating actin/thin filaments in the presence or absence of OM. This fundamental aspect of the hydrolysis mechanism has yet to be determined.

A summary of the rate and equilibrium constants measured for the kinetic mechanism with and without OM is given in Table 2. The relative changes in the rates of the different steps of the mechanism that are altered by OM are shown by the values in parentheses in Figure 9A. ATP rapidly dissociates the actoPV-HMM complex, and the second-order rate constant and maximal rates are reduced by ~30% by OM. The maximal rate of dissociation of ADP from actoPV-HMM-ADP was not altered by the drug. The maximal rate of the ATP hydrolysis step (M-ATP → M-ADP-P_i) is fast and is not significantly affected by OM; however, the equilibrium constant of ATP hydrolysis is increased 2.5-fold from 2.4 to 6, indicating a shift toward product formation (M-ADP-P_i) in the active site. These data indicate that the largest effect of OM is on the rate of the reverse hydrolysis step, ATP synthesis, which is decreased ~2.5-fold. Although OM only modestly (1.6-fold) increases the rate constant of the fast phase of dissociation of phosphate from actomyosin-ADP-P_i, the fraction of the amplitude of the fast phase of phosphate dissociation is increased ~4-fold, which is not consistent with the 20% increase in the fraction of M-ADP-P_i calculated from an increase in K_H from 2.5 to 6 by OM in Figure 5 according to Scheme 1.

Molecular dynamics simulations[36,37] and experimental data[38−40] support the hypothesis that binding of ATP to the active site of myosin promotes coupling of the SH-1 helix, relay helix, and converter domain to produce a rotation in the lever arm position from the down $M_↓$ (near rigor) to up $M_↑$ (prepower stroke) conformation during the recovery stroke in the absence of actin.[41,42] The change in conformation of the myosin is linked to the change in fluorescence emission of tryptophan 508, which is located in the converter. The opposite of this transition occurs upon dissociation of phosphate from $AM_↑ADP$-P_i to $AM_↓$-ADP,

DOI: 10.1021/bi5015166
Biochemistry 2015, 54, 1963−1975

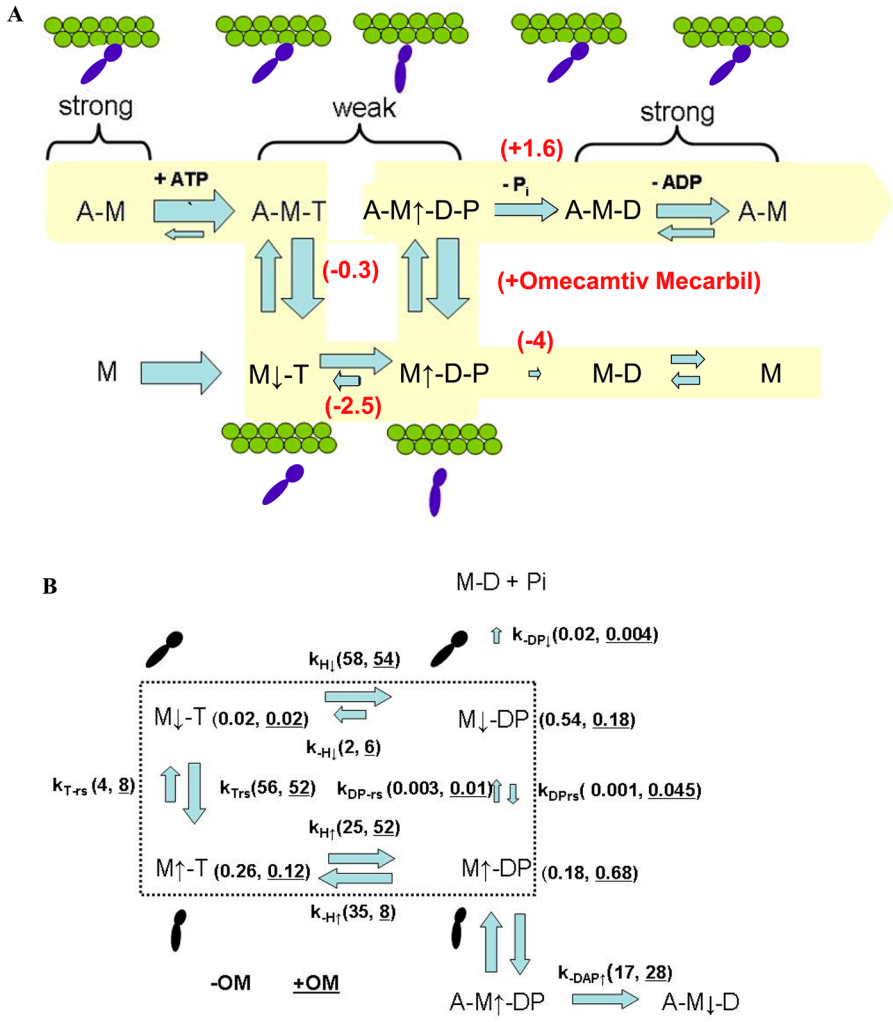

Figure 9. Effect of Omecamtiv Mecarbil on the ATPase mechanism of β-cardiac heavy meromyosin. (A) Cartoon of the actomyosin ATP hydrolysis mechanism. The values in parentheses are the fold increase or decrease in rate constants measured in the presence of Omecamtiv Mecarbil. Abbreviations: A, actin; M, myosin; T, ATP; D, ADP; P, inorganic phosphate. (B) Expanded mechanism of the hydrolysis step in panel A (M↓ATP ⇄ M-ADP-P_i) showing coupled equilibria between ATP hydrolysis and the up (↑) and down (↓) conformations of myosin inside the dashed box. Arrows in the subscripts of the rate constants indicate the conformation of the myosin (i.e., $k_{H\downarrow}$ is the rate of hydrolysis in the down state and $k_{H\uparrow}$ the rate of ATP hydrolysis in the up state). Rate constants for the change from the down (↓) to up (↑) state are given the subscript rs (recovery stroke), while those from up (↑) to down (↓) are indicated by the subscript −rs (reverse recovery stroke). k_{Trs} is the recovery stroke with ATP bound to the active site, and $k_{DP\text{-}rs}$ is the reverse recovery stroke with ADP and P_i bound to the active site. Values in parentheses following the rate constants are the values used in the model described in the Supporting Information for the reaction in the absence and presence of OM. Rate constants used for modeling in the presence of OM are underlined [i.e., $k_{-H\downarrow}$ (2, 6) indicates rate constants of 2 s^{-1} in the absence of OM and 6 s^{-1} in the presence of OM]. The values in parentheses to the right of each intermediate are the fractions of that intermediate calculated for the model. The values calculated in the presence of OM are underlined (i.e., OM increases the fraction of M↑-ADP-P_i from 0.18 to 0.68).

which is associated with the power stroke. Previous models have assumed that the ATP binding to the active site of myosin initiates a recovery stroke that is followed by the hydrolysis step and actin binding. This accelerates phosphate dissociation, which is associated with the power stroke ($M_{\downarrow}$-ATP ↔ $M_{\uparrow}$-ATP ↔ $M_{\uparrow}$-ADP-P_i + actin → $A_{\downarrow}$M-ADP + P_i). We agree that this is the pathway that leads to the power stroke but have expanded the model to allow hydrolysis to occur also before the recovery stroke. In this mechanism, shown in Figure 9B, hydrolysis that occurs prior to the recovery stroke produces a dead end intermediate ($M_{\downarrow}$-ADP-P_i) in which phosphate dissociation is not significantly accelerated by actin. The addition of this dead end intermediate is necessary to provide a consistent explanation for the fluorescence, quenched flow, and phosphate dissociation data in Figures 4, 5, and 7, respectively.

The data in Figures 4, 5, and 7, tryptophan fluorescence, quench flow, and acceleration of phosphate release from myosin-ADP-P_i by actin measure different aspects of the coupled equilibria. The quench flow data in Figure 5 provide a measure of the overall chemical hydrolysis step ([M↓-ATP] + [M↑-ATP]) ⇄ ([M↑-ADP-P_i] + [M↓-ADP-P_i]). The apparent K_H ([M↑-ADP-P_i] + [M↓-ADP-P_i])/([M↓-ATP] + [M↑-ATP]) is increased from 2.4 to 6 by OM. Similarly, an apparent equilibrium constant for the recovery stroke can be measured from the change in tryptophan fluorescence, i.e., ([M↓-ATP] + [M↓-ADP-P_i]) ⇄ ([M↑-ATP] + [M↑-ADP-P_i]). The apparent equilibrium constant for the recovery stroke K_{rs} {([$M_{\uparrow}$-ATP] + [$M_{\uparrow}$-ADP-P_i])/([$M_{\uparrow}$-ATP] + [$M_{\uparrow}$-ADP-P_i])} increases ~2-fold with OM. The maximal rates of the hydrolysis and conformational steps at saturating ATP concentrations

DOI: 10.1021/bi5015166
Biochemistry 2015, 54, 1963−1975

measured either by quench flow or tryptophan fluorescence are similar, and both are unchanged by OM (Figures 4 and 5). The kinetics of phosphate dissociation observed in Figure 7 measure the thin filament-activated dissociation of phosphate from the steady-state mixture of intermediates shown in Figure 9B. Efficient coupling of product dissociation to produce maximal force and work production make it likely that the rapid phosphate dissociation occurs primarily from $AM_{\uparrow}$-ADP-P_i after it has undergone the recovery stroke but not from $AM_{\downarrow}$-ADP-P_i. The slow phases of phosphate dissociation could be from the prerecovery stroke M↓-ADP-P_i intermediate or a result of the re-equilibration of the conformational states and hydrolysis steps after thin filament binding to one or more of the intermediates in Figure 9B. Although all of the rate and equilibrium constants in Figure 9B cannot be unambiguously determined by the available data, the rate and equilibrium constants shown in Figure 9B provide a plausible explanation for several aspects of the data that could not be explained by the minimal mechanism in Scheme 1. Scheme 1 predicts that the amplitude of the fast phase of the phosphate dissociation is directly determined by the equilibrium constant of the hydrolysis step, K_H; however, the data indicate that the fraction of M↑-ADP-P_i increases from 0.7 to 0.85, the fraction of fast phosphate dissociation increases from 0.15 to 0.60, and the fluorescence amplitude increases ∼2-fold. These apparent inconsistencies can be ascribed only if fast phosphate dissociation by actin occurs with $M_{\uparrow}$-ADP-P_i, whereas both $M_{\uparrow}$-ADP-P_i and $M_{\downarrow}$-ADP-P_i contribute to the phosphate burst measured by quench flow.

The fraction of each intermediate in the absence and presence of OM was calculated using the system of differential equations described in the Supporting Information. These fractions were then used to determine the expected amplitudes of the quench flow, tryptophan fluorescence enhancement, and fast phase of phosphate dissociation that are summarized in Table S1 of the Supporting Information. Rate constants were optimized by trial and error until the values calculated by the model were in good agreement with the experimental data as shown in Table S1 of the Supporting Information. The calculated fraction of the M-ADP-P_i intermediates (for [$M_{\downarrow}$-ADP-P_i] + [$M_{\uparrow}$-ADP-P_i], 0.54 + 0.18 = 0.72 in the absence of OM and 0.18 + 0.68 = 0.86 in the presence of OM) agrees within experimental error with the quench flow data in Figure 5. The fractions of the highly fluorescent intermediates, $M_{\uparrow}$-ATP and $M_{\uparrow}$-ADP-P_i (0.26 + 0.18 = 0.44 in the absence and 0.12 + 0.68 = 0.80 in the presence of OM), are in good agreement with the ∼2-fold increase in fluorescence observed in Figure 4D. OM increases the fraction of rapid phosphate dissociation from 0.15 to 0.60 that is in reasonably good agreement with the calculated values of 0.18 and 0.68 obtained by the simulation. The aim here is to demonstrate that such a model is sufficient to explain the data, but we do not claim that it is the best or only fit that can be made.

The increase in the fractional amplitude (f_A) and rate of fast dissociation of phosphate from AM-ADP-P_i, k_{-DAP} (Figure 7), by OM will produce a larger flux through steps of the mechanism leading to crossbridge reattachment and phosphate dissociation. However, OM does not affect the rate of dissociation of ADP from actomyosin that limits unloaded crossbridge detachment, k_{-AD} (Figure 6). The duty ratio (d_{ratio}) calculated using eq 1 is increased from 0.03 to 0.17, and a higher fraction of myosin is expected to be bound to actin in the strong AM-ADP state.

$$d_{ratio} = f_A k_{-DAP}/(f_A k_{-DAP} + k_{-AD}) \quad (1)$$

Because the rate of dissociation of ADP from actomyosin-ADP is not affected by OM in the absence of load, the increase in the concentration of the AM-ADP intermediate will increase the number of force-producing crossbridges. This is consistent with the slowing of actin filament velocity in the *in vitro* motility assay (Figure 8). For PV-HMM, the unloaded shortening velocity is 0.96 μm/s. OM produces a large (∼14-fold) reduction in filament velocity. This can be at least partially explained by a larger number of crossbridges interacting with actin resulting from the increased duty ratio and higher fraction of strong crossbridges induced by OM. Recruiting more crossbridges produces an internal load on the actin filaments slowing the velocity, but this will also result in more force production, a favorable outcome for improving systolic function. This could also lead to a strain-dependent slowing of the ADP dissociation step, an additional mechanism that would contribute to the observed decrease in velocity. Such a strain-dependent step would produce an extended duration of systole as is measured in the animal model with OM,[9] but the magnitude of change is not likely to be as large as observed here by the *in vivo* motility studies.

We conclude that the main kinetic effects of Omecamtiv Mecarbil are a consequence of shifting the equilibrium of the hydrolysis toward M↑-ADP-P_i. This results in a higher concentration of the actomyosin-ADP-P_i intermediate and accelerated phosphate release, resulting in an increase in the duty ratio. The observed decrease in the rate and more consistent movement in motility experiments are the result of more strongly attached crossbridges that reduce the velocity but increase the force. It is also possible, even likely, that the transition that limits motility in the presence of OM is no longer ADP dissociation as OM does not change the rate of ADP dissociation. These results indicate that OM does not function as a myosin ATPase activator to increase velocity but rather is an allosteric effector that increases force production by the heart.

■ ASSOCIATED CONTENT

Supporting Information

Dependence of steady-state ATP hydrolysis upon pCa and OM concentration, characteristic space−time curves for PV-HMM-powered motility of actin filaments, and modeling of the coupled hydrolysis mechanism to determine the steady-state concentrations of intermediates $M_{\downarrow}$ADP-P_i, $M_{\uparrow}$ADP-P_i, $M_{\downarrow}$ATP, and $M_{\uparrow}$ATP. This material is available free of charge via the Internet at http://pubs.acs.org.

■ AUTHOR INFORMATION

Corresponding Author

*Department of Physiological Sciences, Eastern Virginia Medical School, Norfolk, VA 23507. E-mail: forgace@evms.edu. Phone: (757) 446-5108. Fax: (757) 624-2270.

Funding

This work was supported by National Institutes of Health grant (1R56HL124284-01), an American Heart Association grant (12BGIA 12030120), and a Jeffress Memorial Trust Research Grant Award (J-1037) to E.F. and an American Heart Association grant (10GRNT4300022) to D.A.W.

Notes

The authors declare no competing financial interest.

■ ABBREVIATIONS

OM, Omecamtiv Mecarbil; TF, thin filament; PV-HMM, porcine ventricular heavy meromyosin; pCa, calcium concentration as −log[Ca^{2+}]; MDCC-PBP, *N*-[2-(1-maleimidyl)ethyl]-

DOI: 10.1021/bi5015166
Biochemistry 2015, 54, 1963−1975

7-(diethylamino)coumarin-3-carboxamide phosphate-binding protein; P_i, inorganic phosphate; DMSO, dimethyl sulfoxide.

REFERENCES

(1) Liu, L., and Eisen, H. J. (2014) Epidemiology of heart failure and scope of the problem. *Cardiology Clinics 32*, 1−8 , vii.

(2) Tang, W. H., and Francis, G. S. (2010) The year in heart failure. *J. Am. Coll. Cardiol. 55*, 688−696.

(3) Palazzuoli, A., and Nuti, R. (2010) Heart failure: Pathophysiology and clinical picture. *Contrib. Nephrol. 164*, 1−10.

(4) Petersen, J. W., and Felker, G. M. (2008) Inotropes in the management of acute heart failure. *Crit. Care Med. 36*, S106−S111.

(5) Teerlink, J. R., Metra, M., Zaca, V., Sabbah, H. N., Cotter, G., Gheorghiade, M., and Cas, L. D. (2009) Agents with inotropic properties for the management of acute heart failure syndromes. Traditional agents and beyond. *Heart Failure Rev. 14*, 243−253.

(6) Francis, G. S., Bartos, J. A., and Adatya, S. (2014) Inotropes. *J. Am. Coll. Cardiol. 63*, 2069−2078.

(7) Malik, F. I., Hartman, J. J., Elias, K. A., Morgan, B. P., Rodriguez, H., Brejc, K., Anderson, R. L., Sueoka, S. H., Lee, K. H., Finer, J. T., Sakowicz, R., Baliga, R., Cox, D. R., Garard, M., Godinez, G., Kawas, R., Kraynack, E., Lenzi, D., Lu, P. P., Muci, A., Niu, C., Qian, X., Pierce, D. W., Pokrovskii, M., Suehiro, I., Sylvester, S., Tochimoto, T., Valdez, C., Wang, W., Katori, T., Kass, D. A., Shen, Y. T., Vatner, S. F., and Morgans, D. J. (2011) Cardiac myosin activation: A potential therapeutic approach for systolic heart failure. *Science 331*, 1439−1443.

(8) Cleland, J. G., Teerlink, J. R., Senior, R., Nifontov, E. M., McMurray, J. J., Lang, C. C., Tsyrlin, V. A., Greenberg, B. H., Mayet, J., Francis, D. P., Shaburishvili, T., Monaghan, M., Saltzberg, M., Neyses, L., Wasserman, S. M., Lee, J. H., Saikali, K. G., Clarke, C. P., Goldman, J. H., Wolff, A. A., and Malik, F. I. (2011) The effects of the cardiac myosin activator, omecamtiv mecarbil, on cardiac function in systolic heart failure: A double-blind, placebo-controlled, crossover, dose-ranging phase 2 trial. *Lancet 378*, 676−683.

(9) Shen, Y. T., Malik, F. I., Zhao, X., Depre, C., Dhar, S. K., Abarzua, P., Morgans, D. J., and Vatner, S. F. (2010) Improvement of cardiac function by a cardiac Myosin activator in conscious dogs with systolic heart failure. *Circ.: Heart Failure 3*, 522−527.

(10) Lymn, R. W., and Taylor, E. W. (1971) Mechanism of adenosine triphosphate hydrolysis by actomyosin. *Biochemistry 10*, 4617−4624.

(11) Guilford, W. H., Dupuis, D. E., Kennedy, G., Wu, J., Patlak, J. B., and Warshaw, D. M. (1997) Smooth muscle and skeletal muscle myosins produce similar unitary forces and displacements in the laser trap. *Biophys. J. 72*, 1006−1021.

(12) Ishijima, A., Kojima, H., Higuchi, H., Harada, Y., Funatsu, T., and Yanagida, T. (1996) Multiple- and single-molecule analysis of the actomyosin motor by nanometer-piconewton manipulation with a microneedle: Unitary steps and forces. *Biophys. J. 70*, 383−400.

(13) Molloy, J. E., Burns, J. E., Kendrickjones, J., Tregear, R. T., and White, D. C. S. (1995) Movement and Force Produced by a Single Myosin Head. *Nature 378*, 209−212.

(14) Sugiura, S., Kobayakawa, N., Fujita, H., Yamashita, H., Momomura, S., Chaen, S., Omata, M., and Sugi, H. (1998) Comparison of unitary displacements and forces between 2 cardiac myosin isoforms by the optical trap technique: Molecular basis for cardiac adaptation. *Circ. Res. 82*, 1029−1034.

(15) Sommese, R. F., Sung, J., Nag, S., Sutton, S., Deacon, J. C., Choe, E., Leinwand, L. A., Ruppel, K., and Spudich, J. A. (2013) Molecular consequences of the R453C hypertrophic cardiomyopathy mutation on human β-cardiac myosin motor function. *Proc. Natl. Acad. Sci. U.S.A. 110*, 12607−12612.

(16) Malmqvist, U. P., Aronshtam, A., and Lowey, S. (2004) Cardiac myosin isoforms from different species have unique enzymatic and mechanical properties. *Biochemistry 43*, 15058−15065.

(17) Spudich, J. A., and Watt, S. (1971) The regulation of rabbit skeletal muscle contraction. I. Biochemical studies of the interaction of the tropomyosin-troponin complex with actin and the proteolytic fragments of myosin. *J. Biol. Chem. 246*, 4866−4871.

(18) Spiess, M., Steinmetz, M. O., Mandinova, A., Wolpensinger, B., Aebi, U., and Atar, D. (1999) Isolation, electron microscopic imaging, and 3-D visualization of native cardiac thin myofilaments. *J. Struct. Biol. 126*, 98−104.

(19) Matsumoto, F., Makino, K., Maeda, K., Patzelt, H., Maeda, Y., and Fujiwara, S. (2004) Conformational changes of troponin C within the thin filaments detected by neutron scattering. *J. Mol. Biol. 342*, 1209−1221.

(20) Brune, M., Hunter, J. L., Corrie, J. E., and Webb, M. R. (1994) Direct, real-time measurement of rapid inorganic phosphate release using a novel fluorescent probe and its application to actomyosin subfragment 1 ATPase. *Biochemistry 33*, 8262−8271.

(21) Siemankowski, R. F., and White, H. D. (1984) Kinetics of the interaction between actin, ADP and cardiac myosin-S1. *J. Biol. Chem. 259*, 5045−5053.

(22) Forgacs, E., Sakamoto, T., Cartwright, S., Belknap, B., Kovacs, M., Toth, J., Webb, M. R., Sellers, J. R., and White, H. D. (2009) Switch 1 Mutation S217A Converts Myosin V into a Low Duty Ratio Motor. *J. Biol. Chem. 284*, 2138−2149.

(23) White, H. D., Belknap, B., and Webb, M. R. (1997) Kinetics of nucleoside triphosphate cleavage and phosphate release steps by associated rabbit skeletal actomyosin, measured using a novel fluorescent probe for phosphate. *Biochemistry 36*, 11828−11836.

(24) Eccleston, J. F., Hutchinson, J. P., and White, H. D. (2001) Stopped Flow Fluorescence. In *Protein-Ligand Interactions: Structure and Spectroscopy* (Harding, S. E., and Chowdhry, B., Eds.) Oxford University Press, Oxford, U.K.

(25) Bourdieu, L., Magnasco, M. O., Winkelmann, D. A., and Libchaber, A. (1995) Actin filaments on myosin beds: The velocity distribution. *Phys. Rev. E: Stat., Nonlinear, Soft Matter Phys. 52*, 6573−6579.

(26) Barua, B., Winkelmann, D. A., White, H. D., and Hitchcock-DeGregori, S. E. (2012) Regulation of actin-myosin interaction by conserved periodic sites of tropomyosin. *Proc. Natl. Acad. Sci. U.S.A. 109*, 18425−18430.

(27) Wang, Q., Moncman, C. L., and Winkelmann, D. A. (2003) Mutations in the motor domain modulate myosin activity and myofibril organization. *J. Cell Sci. 116*, 4227−4238.

(28) Batra, R., and Manstein, D. J. (1999) Functional characterisation of *Dictyostelium* myosin II with conserved tryptophanyl residue 501 mutated to tyrosine. *Biol. Chem. 380*, 1017−1023.

(29) Park, S., and Burghardt, T. P. (2000) Isolating and localizing ATP-sensitive tryptophan emission in skeletal myosin subfragment 1. *Biochemistry 39*, 11732−11741.

(30) Malnasi-Csizmadia, A., Woolley, R. J., and Bagshaw, C. R. (2000) Resolution of conformational states of *Dictyostelium* myosin II motor domain using tryptophan (W501) mutants: Implications for the open-closed transition identified by crystallography. *Biochemistry 39*, 16135−16146.

(31) Johnson, K. A., and Taylor, E. W. (1978) Intermediate states of subfragment 1 and actosubfragment 1 ATPase: Reevaluation of the mechanism. *Biochemistry 17*, 3432−3442.

(32) Siemankowski, R. F., and White, H. D. (1984) Kinetics of the interaction between actin, ADP, and cardiac myosin-S1. *J. Biol. Chem. 259*, 5045−5053.

(33) Houmeida, A., Heeley, D. H., Belknap, B., and White, H. D. (2010) Mechanism of regulation of native cardiac muscle thin filaments by rigor cardiac myosin-S1 and calcium. *J. Biol. Chem. 285*, 32760−32769.

(34) Greenberg, M. J., Shuman, H., and Ostap, E. M. (2014) Inherent force-dependent properties of β-cardiac myosin contribute to the force-velocity relationship of cardiac muscle. *Biophys. J. 107*, L41−L44.

(35) Wang, Y., Ajtai, K., and Burghardt, T. P. (2014) Analytical comparison of natural and pharmaceutical ventricular myosin activators. *Biochemistry 53*, 5298−5306.

(36) Baumketner, A. (2012) The mechanism of the converter domain rotation in the recovery stroke of myosin motor protein. *Proteins 80*, 2701−2710.

DOI: 10.1021/bi5015166
Biochemistry 2015, 54, 1963−1975

(37) Fischer, S., Windshugel, B., Horak, D., Holmes, K. C., and Smith, J. C. (2005) Structural mechanism of the recovery stroke in the myosin molecular motor. *Proc. Natl. Acad. Sci. U.S.A. 102*, 6873−6878.
(38) Koppole, S., Smith, J. C., and Fischer, S. (2007) The structural coupling between ATPase activation and recovery stroke in the myosin II motor. *Structure 15*, 825−837.
(39) Kintses, B., Yang, Z., and Malnasi-Csizmadia, A. (2008) Experimental investigation of the seesaw mechanism of the relay region that moves the myosin lever arm. *J. Biol. Chem. 283*, 34121−34128.
(40) Urbanke, C., and Wray, J. (2001) A fluorescence temperature-jump study of conformational transitions in myosin subfragment 1. *Biochem. J. 358*, 165−173.
(41) Agafonov, R. V., Negrashov, I. V., Tkachev, Y. V., Blakely, S. E., Titus, M. A., Thomas, D. D., and Nesmelov, Y. E. (2009) Structural dynamics of the myosin relay helix by time-resolved EPR and FRET. *Proc. Natl. Acad. Sci. U.S.A. 106*, 21625−21630.
(42) Muretta, J. M., Petersen, K. J., and Thomas, D. D. (2013) Direct real-time detection of the actin-activated power stroke within the myosin catalytic domain. *Proc. Natl. Acad. Sci. U.S.A. 110*, 7211−7216.

DOI: 10.1021/bi5015166
Biochemistry 2015, 54, 1963−1975